

Highlights

Modeling the Impact of Iron Defect Variability on Silicon Solar Cell Performance Across Different Scenarios

Oleg Olikh,Oleksii Zavhorodnii

- 1
- 2
- 3

Modeling the Impact of Iron Defect Variability on Silicon Solar Cell Performance Across Different Scenarios

Oleg Olikh*, Oleksii Zavhorodnii

Taras Shevchenko National University of Kyiv, 64/13, Volodymyrska Street, Kyiv, 01601, Ukraine

ARTICLE INFO

Keywords:
silicon
iron-boron pairs
solar cells
SCAPS
simulation
defect influence

ABSTRACT

1. Introduction

The necessity for renewable energy sources to meet the growing global demand for sustainable and environmentally friendly energy alternatives has become evident. Among the wide range of renewable energy sources, sunlight is the cleanest, safest, and most abundant source for use in sustainable energy to support economic growth [1]. The utilization of solar energy heavily depends on the use of photovoltaic cells, with silicon-based devices playing a critical role [2, 3].

The issue of semiconductor purity has become increasingly significant since the advent of the transistor in 1947 [4]. The 1960 study by Shockley and Queisser [5] demonstrated that the electrical properties of $n^+ - p$ silicon diodes deteriorate when impurity atoms of metals such as Cu, Fe, Mn, Au, Zn, and Ni are present. This study prompted investigations focused on preventing contaminating metals from entering semiconductors during manufacturing. In particular, metallic impurities are known to reduce the efficiency of silicon-based devices through direct shunting [6], increased leakage current [7], or bulk recombination [8]. Despite extensive study of metallic impurities in silicon over the past fifty years [4, 9], the problem continues to attract significant attention [10, 11, 12, 13, 14].

Iron is prominent among metallic contaminants, with its atoms being among the most prevalent and detrimental impurities in silicon solar cells (SSCs) [15]. Even in small concentrations (about 10^{10} cm $^{-3}$), point defects related to Fe can significantly influence the performance of SSCs [16, 17]. Therefore, it is of critical importance to assess the concentration of iron impurities. In response to this challenge, various methodologies have been put forward, often based on the property of iron atoms to form pairs with acceptors. In particular, iron atoms are predominantly located in interstitial positions in silicon, forming the Fe_i defect. In *p*-type crystals, without external illumination, iron atoms carry positive charges and tend to bond with negatively charged doping atoms (boron, aluminum, gallium, or indium), forming $\text{Fe}_i\text{B}_{\text{Si}}$ pairs [18]. However, these pairs can destabilized by intense illumination, electron injection, or heating up to 200 °C [19]. The recombination properties of iron-related defects Fe_i and Fe_iB_s differ significantly, which profoundly affects the overall characteristics of the crystal. This fact formed the basis for the first method of assessing iron concentration [20], which relied on measuring the diffusion length of minority carriers using the surface photovoltage method [21]. Many other methods involve measurements of carrier lifetime [22, 23], Quasi-Steady-State Photoconductance [24], or the study of kinetic dependencies of short-circuit current [25] or photoluminescence intensity [26] during the reaction $\text{Fe}_i\text{B}_{\text{Si}} \rightleftharpoons \text{Fe}_i + \text{B}_{\text{Si}}$.

Notably, the presence of Fe-related defects affects the dynamics of electron and hole movement within the solar cell, which is reflected in changes to the appearance of the current–voltage (I - V) characteristics of SSCs overall, as well as modifications to the main photoelectric parameters (short-circuit current I_{SC} , open-circuit voltage V_{OC} , efficiency η , and fill factor FF) in particular. These findings create fundamental possibilities to advance methods for estimating iron concentration by I - V curves measuring before and after pair dissolution. The advantages of such an approach are associated with the possibility of directly characterizing finished solar cells, as well as the absence of the need for additional equipment other than that required for I - V measurements, which is extremely common. Efforts have been made initially in developing such methods. For instance, it was proposed to estimate the concentration of iron in SSCs

 olegolikh@knu.ua (O. Olikh); nevermor464@gmail.com (O. Zavhorodnii)
ORCID(s): 0000-0003-0633-5429 (O. Olikh); 0000-0001-8080-7661 (O. Zavhorodnii)

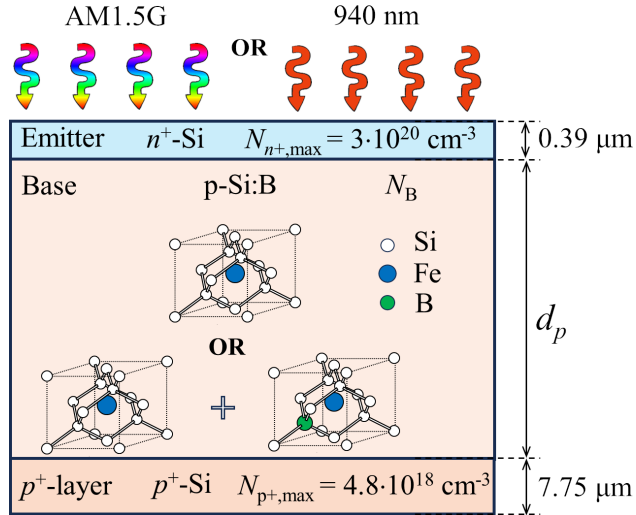


Figure 1: Schematic diagram of analyzed solar cells.

based on changes in the ideality factor [27, 28] or open-circuit voltage [17]. However, developing such approaches requires evaluating how a particular parameter changes when iron-containing pairs dissolve and determining whether it can estimate the iron concentration N_{Fe} . For example, the most evident conditions for utilizing a specific parameter include its change due to the transformation $\text{Fe}_i\text{B}_{\text{Si}} \rightarrow \text{Fe}_i + \text{B}_{\text{Si}}$, at least by 10 %, along with a monotonic dependence of these changes on N_{Fe} .

This paper intends to determine the variations of I_{SC} , V_{OC} , η , and FF resulting from the decay of iron-containing pairs in boron-doped silicon solar cells. Previous similar calculations have been conducted [29, 16, 10], but the results presented typically pertain only to certain temperatures, illumination levels (often AM1.5), and solar cells with specific parameters. In this study, we performed calculations over a sufficiently wide temperature range (290–340 K) and for solar cells with varying base thickness (180–380 μm) and doping levels (boron concentration in the base ranging from 10^{15} to 10^{17} cm^{-3}). The results obtained allow us to assess the feasibility and potential of using the main photovoltaic parameters of specific solar cells to estimate the N_{Fe} value across a range of temperatures, including conditions similar to those encountered in typical SSC applications. Furthermore, investigations have explored changes in photoelectric performance under not only solar illumination (AM1.5G) but also low-intensity monochromatic light (wavelength of 940 nm, intensities of 5 W/m² and 10 W/m²). In the first case, while it is customary to adhere to standard conditions, it's essential to consider that illumination at 1000 W/m² can lead to the decay of Fe_iB_s complexes [30]. Therefore, measurements for cases requiring the presence of undissociated pairs in silicon must meet specific constraints. On the other hand, intentionally chosen monochromatic illumination penetrates the emitter with negligible losses and does not reach the rear side. In this context, the photoelectric parameters show remarkable sensitivity to recombination processes occurring within the solar cell base and to iron concentration in this region. Finally, in our calculations, we attempted to use the latest literature data concerning the exact values of silicon parameters, including light absorption values [31] and coefficients characterizing intrinsic recombination [32, 33].

2. Research Methodology

2.1. Simulation Details

The study involved simulation I - V curves of SSCs with an $n^+ - p - p^+$ structure, as illustrated in Fig. 1. A back surface field (p^+ -layer) is a notable feature observed in both Al-BSF cells (full area), which are gradually losing relevance, and PERC cells (locally), which are the most widely used in mass production. The structures with a base uniformly doped with boron were under consideration. The doping concentration N_B , and the base thickness d_p were varied during the modeling process, as detailed in Table 1. The emitter and p^+ -layer were considered to be unevenly doped. The concentration profiles of the dopants, their maximum values ($N_{p^+,max}$ and $N_{n^+,max}$), and layer thicknesses (see Fig. 1) were selected according to Fell et al. [34].

Table 1
Parameters varied during the simulation

Parameter	Range of values
d_p (μm)	180 – 380
N_B (cm^{-3})	$10^{15} – 10^{17}$
N_{Fe} (cm^{-3})	$10^{10} – 10^{14}$
T (K)	290 – 340
Illumination	AM1.5G, 1000 W/m ² ; 940 nm, 5 W/m ² ; 940 nm, 10 W/m ²

The simulation was conducted using the SCAPS 3.3.11 code [35]. SCAPS-1D software, developed by the University of Gent, is founded on theoretical computations that involve solving Poisson's equation, continuity equations for holes and electrons, and drift-diffusion at each position within the solar cell, considering the boundary conditions. Despite its one-dimensional modeling approach, SCAPS is extensively used for modeling various types of solar cells [36, 37, 38, 39] in general and for investigating the effects of defects on their performance [40, 41, 42] in particular.

As can be seen from Table 1, calculations spanned a broad range of temperatures and base doping levels. Therefore, to improve the accuracy of the calculations when inputting the initial parameters into SCAPS, temperature and concentration (where applicable) dependencies of the following silicon parameters were taken into account:

- bandgap according to Passler [43];
- doping induced bandgap narrowing according to Yan & Cuevas [44];
- effective density of states at conduction and valence band and intrinsic carrier concentration according to Couderc et al. [45];
- thermal carrier velocities according to Green [46];
- free carrier effective masses according to O'Mara et al. [47];
- carrier mobilities according to Klaassen's theory [48];

The values of surface recombination coefficients were considered equal to the thermal velocities of carriers [34]. The calculations addressed recombination processes within the structural volume, incorporating both intrinsic recombination and Shockley-Read-Hall recombination at iron-related defects. In the first case, processes of band-to-band radiation recombination were considered (where the calculation of the corresponding coefficient included the fraction of radiatively emitted photons reabsorbed via band-to-band processes according to Niewelt et al.[32]) and Auger recombination (where the coefficients considered the effect of Coulomb enhancement [33] and temperature dependence [49]).

When accounting for the influence of iron impurities, we considered that Fe atoms were uniformly distributed within the base and p^+ -layer with a total concentration of N_{Fe} (see Table 1). Two cases were under consideration:

Case 1. The concentration of interstitial iron defects $[\text{Fe}_i] = N_{\text{Fe}}$ at each position throughout the solar cell, with no pairs present $[\text{Fe}_i\text{B}_s] = 0$. This case corresponds to the state of the structure immediately after intense illumination, for example.

Case 2. Iron atoms predominantly form pairs with acceptors, $[\text{Fe}_i\text{B}_s] \gg [\text{Fe}_i]$, but the exact concentration ratio depends on the position of the Fermi level and temperature [50, 51] and varies from point to point within the solar cell. Further details about calculation of the concentration profiles of Fe_iB_s and Fe_i are provided in [28, 27]. This case corresponds to prolonged storage of the structure in darkness or under conditions of low-intensity ($< 0.01 \text{ J cm}^{-2}$ [30]) illumination.

During the calculations, it was assumed that Fe_i forms a single donor level, while the Fe_iB_s pair has a trigonal configuration and acts as an amphoteric defect. We obtained defect parameters (including level positions within the bandgap and electron and hole capture cross-sections) from relevant studies [52, 53, 54].

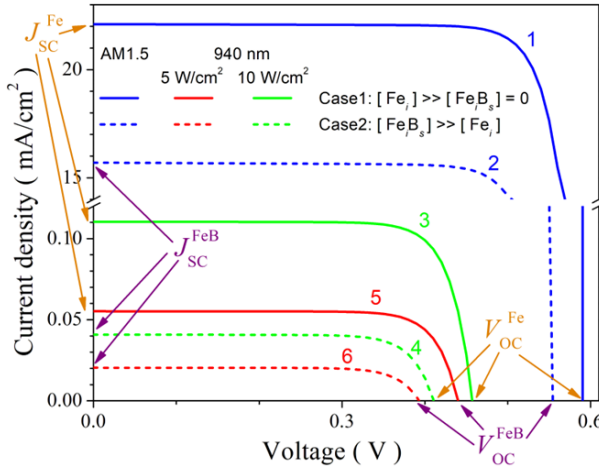


Figure 2: Typical IV characteristics, calculated for structure with $d_p = 180 \mu\text{m}$, $N_B = 10^{17} \text{ cm}^{-3}$, $N_{\text{Fe}} = 10^{14} \text{ cm}^{-3}$ at $T = 290 \text{ K}$. Illumination: AM1.5 (curves 1, 2), 940 nm 10 Wcm^{-2} (3, 4) and 940 nm 5 Wcm^{-2} (5, 6). Solid and dotted lines correspond to Case 1 and Case 2, respectively.

As previously mentioned, the solar cell behavior was simulated under different illumination conditions, including solar light (AM1.5G) and monochromatic light (wavelength 940 nm, intensity of $W_{\text{ill}} = 5 \text{ Wm}^{-2}$ or 10 W/m^2) — see Table 1. The calculations incorporated the light absorption values in silicon based on Green's study [31].

The I - V characteristics were simulated for both Case 1 and Case 2 (see Fig. 2), and from each curve, the short-circuit current, open-circuit voltage, efficiency, and fill factor were determined. Assessing the influence of iron defect variability relied on the relative changes in each photovoltaic conversion parameter:

$$\varepsilon A = \frac{A^{\text{FeB}} - A^{\text{Fe}}}{A^{\text{FeB}}} \times 100\%, \quad (1)$$

where A represents one of the parameters (I_{SC} , V_{OC} , η , and FF), superscript "FeB" corresponds to the parameter value for coexistence of Fe_i and Fe_iB_s (Case 2), superscript "Fe" is related to the decay of all pairs (Case 1).

Impact of change of iron defects was investigated as a function of temperature from 290 K to 340 K, base depth from $180 \mu\text{m}$ to $380 \mu\text{m}$, base doping level from 10^{15} cm^{-3} to 10^{17} cm^{-3} , and total impurity iron atom concentration from 10^{10} cm^{-3} to 10^{14} cm^{-3} . For each illumination scenario, calculations were carried out with 11 different temperature values and 5 base depth values, evenly distributed within the specified ranges. The concentration values were distributed equally on a logarithmic scale with 4 (N_B case) and 6 (N_{Fe} case) steps per decade. As a result, for the AM1.5 illumination scenario, for instance, 24750 I - V characteristics were simulated. An exception occurred with monochromatic illumination at $W_{\text{ill}} = 10 \text{ Wm}^{-2}$, where we used only two d_p values.

2.2. Experimental Details

To evaluate the validity of the simulated results, we also conducted experimental studies on the effect of changing the state of iron-related defects on the photoelectric parameters of silicon solar cells.

The n^+ - p^+ -Si samples were used in the experiment. The structure was fabricated from a $380 \mu\text{m}$ thick p -type boron-doped Czochralski silicon (100) wafer with doping level $N_B = 1.36 \times 10^{15} \text{ cm}^{-3}$. The n^+ emitter with a sheet resistance of about $20 - 30 \Omega/\square$ and thickness of $0.7 \mu\text{m}$ was formed by phosphorus diffusion. The anti-recombination isotype barrier was created by using a p^+ layer ($10 - 20 \Omega/\square$) formed by boron diffusion. On the front surface, SiO_2 (40 nm) and Si_3N_4 (30 nm) films were formed as antireflective and passivating layers, respectively. The solid and grid Al contacts were formed by magnetron sputtering on the back and front surfaces, respectively.

The I - V characteristics were measured using a Keithley 2450 source meter and low-intensity monochromatic light source (light-emitting diode SN-HPIR940nm-1W with light wavelength 940 nm and intensity of about $W_{\text{ill}} = 5 \text{ Wm}^{-2}$).

For different samples, the iron concentration ranged from 2×10^{11} to $4 \times 10^{13} \text{ cm}^{-3}$. The values of N_{Fe} were determined using a methodology [55, 25], based on fitting the kinetics of short-circuit current. The decay of Fe_iB_s pairs was realized using intensive (7000 W/m^2) halogen lamp illumination.

The measurements were carried over the temperature range of 300–340 K. The sample temperature was driven by a thermoelectric cooler controlled by an STS-21 sensor and maintained constant by a PID algorithm embedded in the software that serves the experimental setup.

3. Results and Discussion

3.1. Short-circuit current

Figure 3 illustrates the characteristic dependencies of short-circuit current variations resulting from the reconfiguration of iron-containing defects, as obtained from the simulations. We present a more comprehensive set of figures that depict the detailed dependencies of $\varepsilon I_{\text{SC}}$ on all parameters varied during the calculations in the Supplementary Material (Figs. S1–S6). It is important to note that the qualitative nature of the short-circuit current variations remains practically identical under both solar and monochromatic illumination, with the quantitative parameters of $\varepsilon I_{\text{SC}}$ differing: at 940 nm, the absolute values of $\varepsilon I_{\text{SC}}$ are approximately 3–4 times greater than those observed under AM1.5 conditions, assuming other parameters are constant. Among other features of $\varepsilon I_{\text{SC}}$ changes, we can highlight the following:

- The module $\varepsilon I_{\text{SC}}$ increases monotonically with increasing iron concentration, but the sign of this value depends on the doping level. At low boron concentrations ($N_B = 10^{15} \text{ cm}^{-3}$) $\varepsilon I_{\text{SC}} > 0$, whereas at high concentrations ($N_B = 10^{17} \text{ cm}^{-3}$) $\varepsilon I_{\text{SC}} < 0$ - see Figs. 3a, 3c, S3–S6;
- Increasing the acceptor concentration causes a monotonic decrease in $\varepsilon I_{\text{SC}}$ (Figs. 3b, 3d); the N_B value at which the sign of $\varepsilon I_{\text{SC}}$ changes depends on the temperature (decreases with decreasing in T value) and the type of illumination (is generally higher in the case of monochromatic light) — see Fig. S2;
- In the case where $\varepsilon I_{\text{SC}} < 0$, an temperature increase causes a decrease in the absolute magnitude of the relative changes in short-circuit current, with the dependence being nearly linear and the slope increasing with higher doping levels and iron concentration (Figs. 3a, 3c, S4). In the case where $\varepsilon I_{\text{SC}} > 0$, a T changing results in minor non-monotonic variations of the short-circuit current after the dissociation of Fe_iB_s pairs (Fig. S3);
- The influence of base thickness on $\varepsilon I_{\text{SC}}$ increases with increasing N_B and decreasing N_{Fe} (Figs. S5, S3), but it is minimal overall. As calculations have shown, increasing d_p by more than twice causes changes in $\varepsilon I_{\text{SC}}$ that do not exceed 0.5 %;
- Changing the intensity of the monochromatic illumination (from 5 W/m^2 to 10 W/m^2) does not practically change the value of $\varepsilon I_{\text{SC}}$;
- The absolute values of $\varepsilon I_{\text{SC}}$ can reach relatively high values (more than 100 % for 940 nm illumination); however, in cases where $N_{\text{Fe}} < 10^{11} \text{ cm}^{-3}$ and around $N_B = 10^{16} \text{ cm}^{-3}$, the changes in short-circuit current do not exceed a few percent;

The identified features of the $\varepsilon I_{\text{SC}}$ changes can be explained by considering the main reasons for the influence of factors, which varied during simulation, on the photovoltaic conversion. It is known [56] that the main influence of metal impurities on solar cell performance is caused by their effect on the collection efficiency (CE, portion of excess carriers that reach the depletion region of $p-n$ junction). Neglecting the influence of series and shunt resistances, the short-circuit current coincides with the photocurrent I_{ph} , which equals the CE multiplied by the number of light-induced excess carriers. In turn, the CE efficiency can be calculated as a convolution of generation function, which is proportional to $\exp(-\alpha z)$ where α is the absorption coefficient and z is the coordinate along the axis directed perpendicular to the $p-n$ junction from the emitter; and the collection probability, which can be obtained as a solution of homogeneous diffusion equation.

[56, 57]

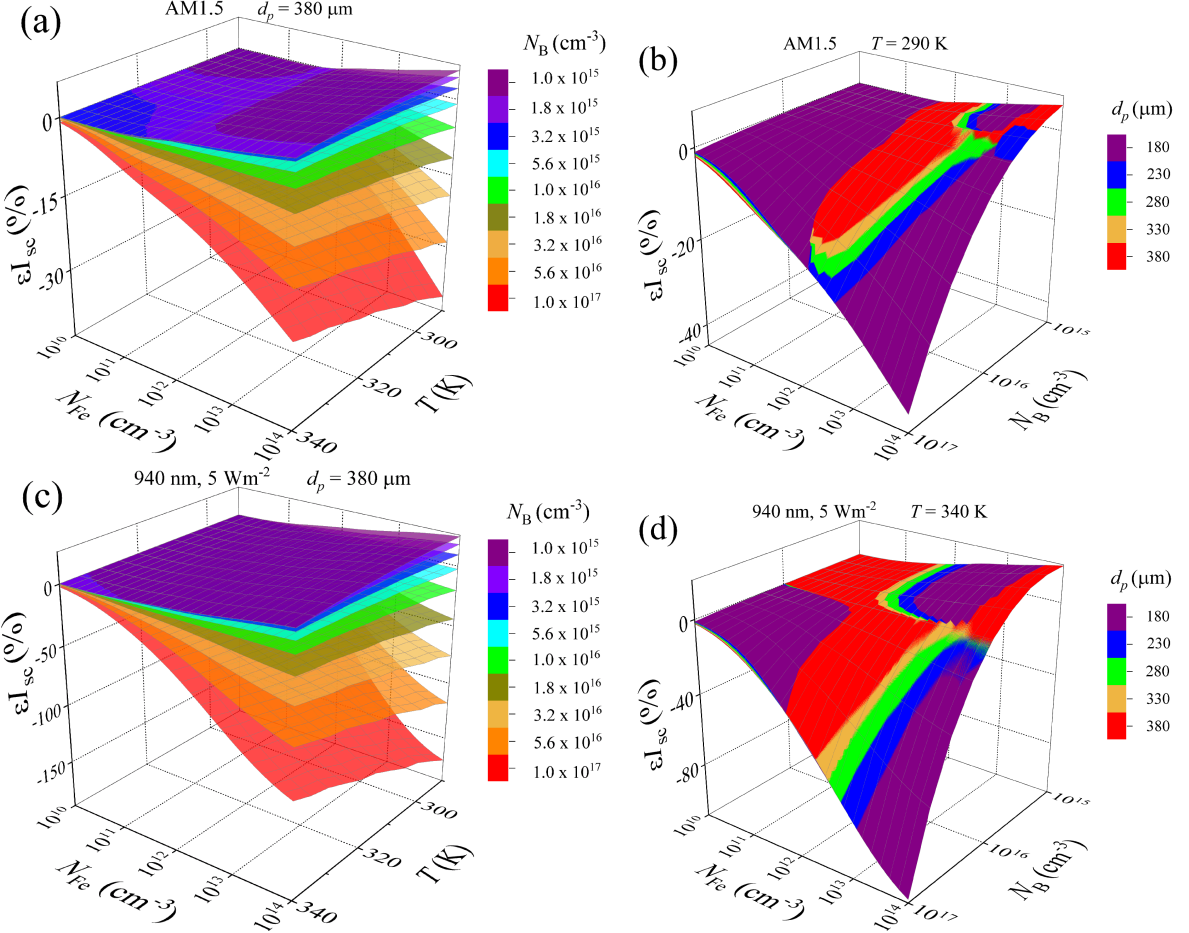


Figure 3: Relative changes in short-circuit current caused by a complete dissociation of Fe_iB_s pairs as a function of iron concentration and temperature (panels a and c) or doping level (b, d). Illumination: AM1.5 (a, b), 940 nm 5 W m^{-2} (c, d). $T, \text{ K}$: 290 (b), 340 (d). Different surfaces correspond to different doping levels (a, c) and base depths (b, d).

3.2. Open-circuit voltage

3.3. Fill factor

The fill factor is another defining term in the overall behavior of a solar cell. FF is the ratio of the maximum obtainable power to the product of short circuit current and open-circuit voltage. In general, FF depends on both I_{SC} and V_{OC} . However, it can be shown that it is mainly determined by the V_{OC} value. Indeed, it is shown [56] within the single-diode model

$$FF \approx \frac{v_{\text{OC}} - \ln(1 + v_{\text{OC}})}{v_{\text{OC}} + 1}, \quad (2)$$

with v_{OC} being the normalized open-circuit voltage $v_{\text{OC}} = qV_{\text{OC}}/nkT$. Another well-known empirical relation for the maximum achievable fill factor of a solar cell is proposed by Green [58, 59]:

$$FF \approx \frac{v_{\text{OC}} - \ln(0.72 + v_{\text{OC}})}{v_{\text{OC}} + 1}. \quad (3)$$

Thus, all factors changing V_{OC} lead also to FF change. However, V_{OC} is present in both the numerator and denominator of Eqs. (2)-(3), and therefore, the expected changes in the fill factor compared to the open-circuit should be smaller.

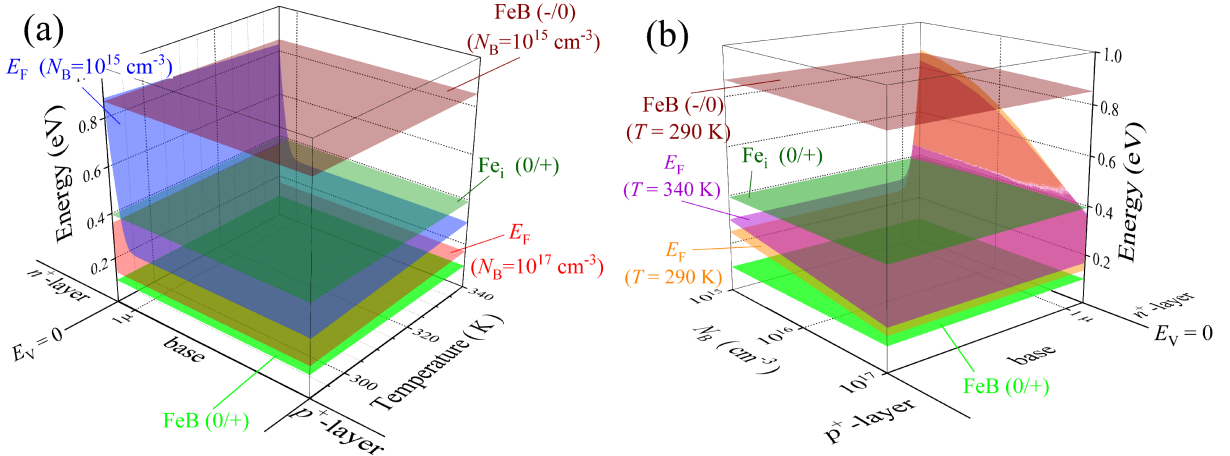


Figure 4: The location of the Fermi level in the base of the n^+ - p - p^+ structure as a function of temperature for $N_B = 10^{15} \text{ cm}^{-3}$ and 10^{17} cm^{-3} (a), and as a function of the doping level for $T = 290$ and 340 K (b). The zero energy value corresponds to the top of the valence band. Also shown are the locations of the donor ($0/+$) levels for the FeB pair (green surfaces) and the interstitial iron atom Fe_i (olive surfaces) and acceptor (-/0) level for FeB pair (brown surfaces).

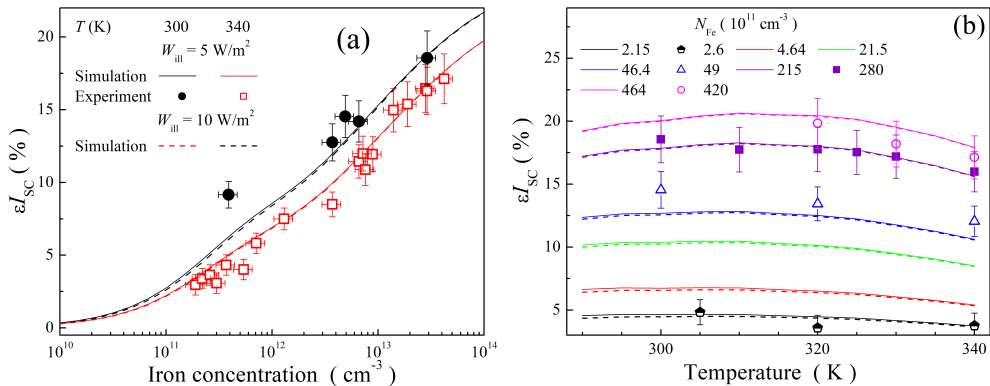


Figure 5: Relative changes in short-circuit caused by a complete dissociation of Fe_iB_s pairs as a function of iron concentration (a) and temperature (b) for SSC with $d_p = 380 \mu\text{m}$ and $N_B = 1.36 \times 10^{15} \text{ cm}^{-3}$ in the case of monochromatic (940 nm) illumination. The marks are the experimental results (divided by factor $C_{cor} = 1.4$), the lines are the simulation results. W_{ill} , Wm^{-2} : 5 (marks and solid lines), 10 (dotted lines). Different lines and marks correspond to different temperatures (a) or N_{Fe} values (b) — see legends.

Recently, Bothe et al. [60] suggested explicit expressions for the FF regarding other characteristic solar cell parameters. Specifically, for p -type SSCs and intrinsic limits, the parameterization can be written as follows:

$$FF = \frac{90.4924}{d_p^{0.00220}} \left[0.9478 + \frac{0.0519}{1 + \left(\frac{\log N_B}{17.3739 d_p^{-0.0093}} \right)^{76.3}} \right], \quad (4)$$

where d_p is expected to be in μm . Additional recombination (e.g., Shockley–Read–Hall) leads to a decrease in FF value [60].

(short-circuit current I_{SC} , open-circuit voltage V_{OC} , efficiency η , and fill factor FF)

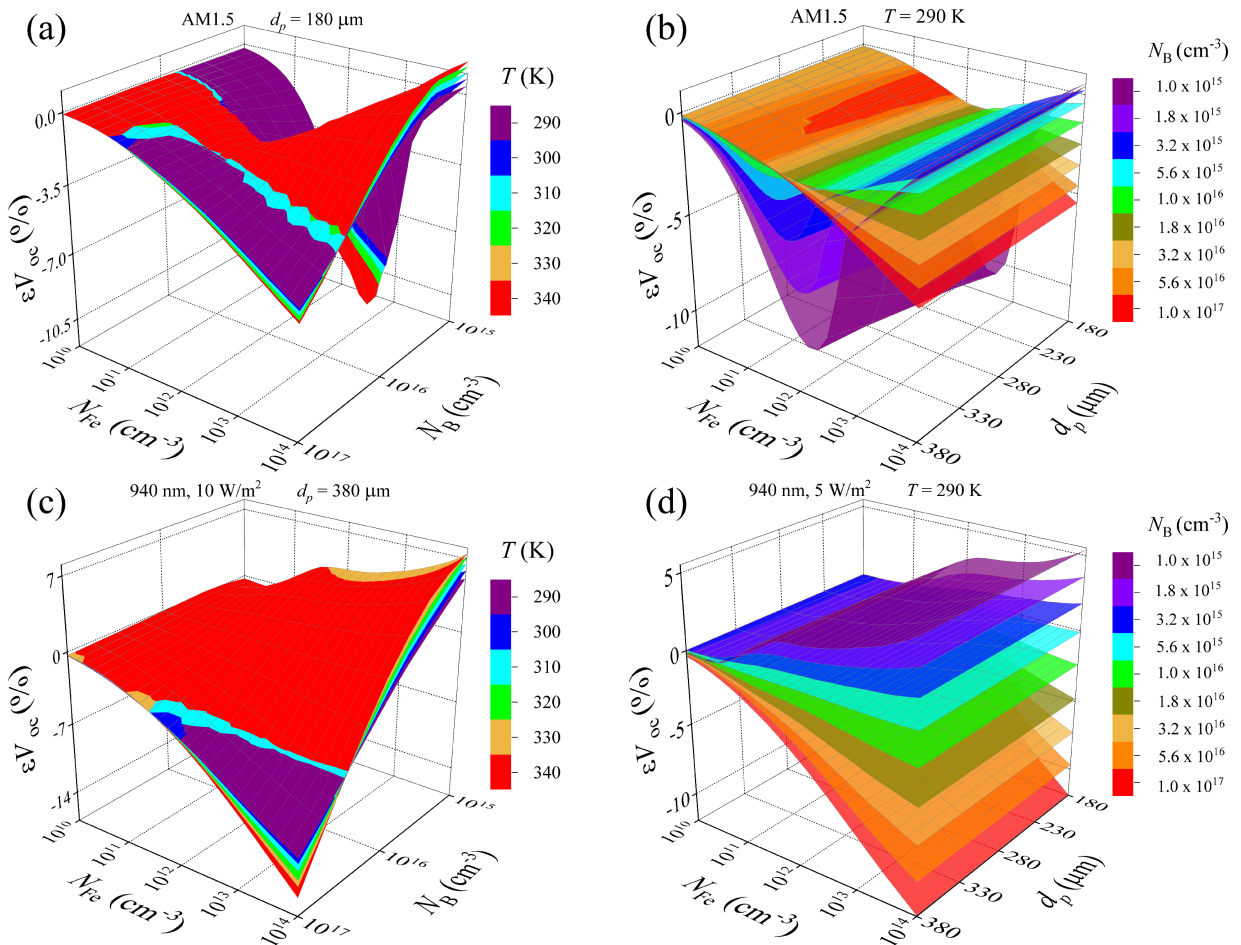


Figure 6: Relative changes in open-circuit voltage caused by a complete dissociation of Fe_iB_s pairs as a function of iron concentration and doping level (panels a and c) or base depth (b, d). Illumination: AM1.5 (a, b), 940 nm 10 W m^{-2} (c), 940 nm 5 W m^{-2} (d). T, K : 290 (b, d). Different surfaces correspond to different temperatures (a, c) and doping levels (b, d).

3.4. Solar Cell Efficiency

4. Conclusion

Acknowledgments

The author (O.O.) would like to acknowledge the financial support by National Research Foundation of Ukraine (Project No. 2023.03/0252 “Development of principles for the creation and machine-oriented characterization of porous silicon nanostructures with optimal heat transport properties”)

Supplementary data

Supplementary data to this article can be found online at <http://surl.li/udqju>

Data availability

Data will be made available on request.

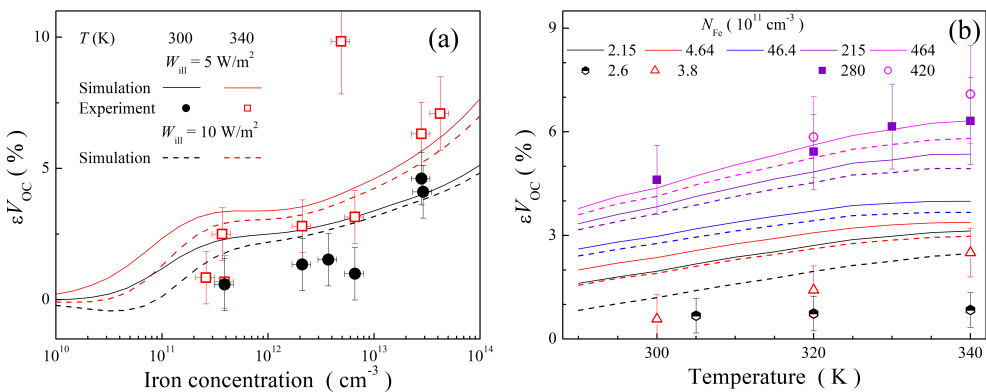


Figure 7: Relative changes in open-circuit voltage caused by a complete dissociation of Fe_iB_s pairs as a function of iron concentration (a) and temperature (b) for SSC with $d_p = 380 \mu\text{m}$ and $N_{\text{B}} = 1.36 \times 10^{15} \text{ cm}^{-3}$ in the case of monochromatic (940 nm) illumination. The marks are the experimental results, the lines are the simulation results. W_{ill} , W m^{-2} : 5 (marks and solid lines), 10 (dotted lines). Different lines and marks correspond to different temperatures (a) or N_{Fe} values (b) — see legends.

References

- [1] B. P. Singh, S. K. Goyal, S. S. A., Grid connected-photovoltaic system (gc-pvs): Issues and challenges, IOP Conference Series: Materials Science and Engineering 594 (2019) 012032.
- [2] R. Basnet, D. Yan, D. Kang, M. M. Shehata, P. Phang, T. Truong, J. Bullock, H. Shen, D. Macdonald, Current status and challenges for hole-selective poly-silicon based passivating contacts, Appl. Phys. Rev. 11 (2024) 011311.
- [3] L. Wang, J. Liu, Y. Li, G. Wei, Q. Li, Z. Fan, H. Liu, Y. An, C. Liu, J. Li, Y. Fu, Q. Liu, D. He, Dislocations in crystalline silicon solar cells, Advanced Energy and Sustainability Research 5 (2024) 2300240.
- [4] C. Claeys, E. Simoen, Metal Impurities in Silicon- and Germanium-Based Technologies: Origin, Characterization, Control, and Device Impact, volume 270 of *Springer Series in Materials Science*, Springer International Publishing, Berlin/New York, 2018.
- [5] A. Goetzberger, W. Shockley, Metal Precipitates in Silicon p-n Junctions, J. Appl. Phys. 31 (1960) 1821–1824.
- [6] O. Breitenstein, J. P. Rakotonaina, M. H. Al Rifai, M. Werner, Shunt types in crystalline silicon solar cells, Prog. Photovolt.: Res. Appl. 12 (2004) 529–538.
- [7] K. Lee, A. Nussbaum, The influences of traps on the generation-recombination current in silicon diodes, Solid-State Electron. 23 (1980) 655–660.
- [8] A. A. Istratov, H. Hieslmair, E. Weber, Iron contamination in silicon technology, Appl. Phys. A 70 (2000) 489–534.
- [9] C. W. Pearce, R. G. McMahon, Role of metallic contamination in the formation of “saucer” pit defects in epitaxial silicon, J. Vac. Sci. Technol. 14 (1977) 40–43.
- [10] A. Hajjiah, M. Soha, I. Gordon, J. Poortmans, J. John, The impact of interstitial fe contamination on n-type cz-silicon for high efficiency solar cells, Sol. Energ. Mat. Sol. 211 (2020) 110550.
- [11] T. T. Le, Z. Zhou, A. Chen, Z. Yang, F. Rougier, D. Macdonald, A. Liu, Reassessing iron–gallium recombination activity in silicon, J. Appl. Phys. 135 (2024) 133107.
- [12] M. Maoudj, D. Bouhafs, N. E. Bourouba, A. Hamida-Ferhat, A. El Amrani, Study of the electrical properties of <100> cz p-type solar-grade silicon wafers against the high-temperature processes, Appl. Phys. A 127 (2021) 407.
- [13] O. Olikh, O. Datsenko, S. Kondratenko, Influence of illumination spectrum on dissociation kinetics of iron–boron pairs in silicon, Phys. Status Solidi A n/a (2024) 2400351.
- [14] H. S. Laine, V. Vähäniemi, A. E. Morishige, J. Hofstetter, A. Haarahiltunen, B. Lai, H. Savin, D. P. Fenning, Impact of iron precipitation on phosphorus-implanted silicon solar cells, IEEE Journal of Photovoltaics 6 (2016) 1094–1102.
- [15] T. Buonassisi, A. A. Istratov, M. D. Pickett, M. Heuer, J. P. Kalejs, G. Hahn, M. A. Marcus, B. Lai, Z. Cai, S. M. Heald, Chemical natures and distributions of metal impurities in multicrystalline silicon materials, Prog. Photovolt.: Res. Appl. 14 (2006) 513–531.
- [16] M. Schubert, M. Padilla, B. Michl, L. Mundt, J. Giesecke, J. Hohl-Ebinger, J. Benick, W. Warta, M. Tajima, A. Ogura, Iron related solar cell instability: Imaging analysis and impact on cell performance, Sol. Energy Mater. Sol. Cells 138 (2015) 96–101.
- [17] A. Herguth, Quantification of iron in boron-doped silicon solar cells from open circuit voltage measurements, IEEE J. Photovolt. 12 (2022) 937–947.
- [18] L. Kimerling, J. Benton, Electronically controlled reactions of interstitial iron in silicon, Physica B+C 116 (1983) 297–300.
- [19] C. Möller, T. Bartel, F. Gibaja, K. Lauer, Iron–boron pairing kinetics in illuminated p-type and in boron/phosphorus co-doped n-type silicon, J. Appl. Phys. 116 (2014) 024503.
- [20] G. Zoth, W. Bergholz, A fast, preparation-free method to detect iron in silicon, J. Appl. Phys. 67 (1990) 6764–6771.
- [21] J. Toušek, J. Toušková, A novel approach to the surface photovoltage method, Sol. Energy Mater. Sol. Cells 92 (2008) 1020–1024.
- [22] S. Rein, S. W. Glunz, Electronic properties of interstitial iron and iron–boron pairs determined by means of advanced lifetime spectroscopy, J. Appl. Phys. 98 (2005) 113711.

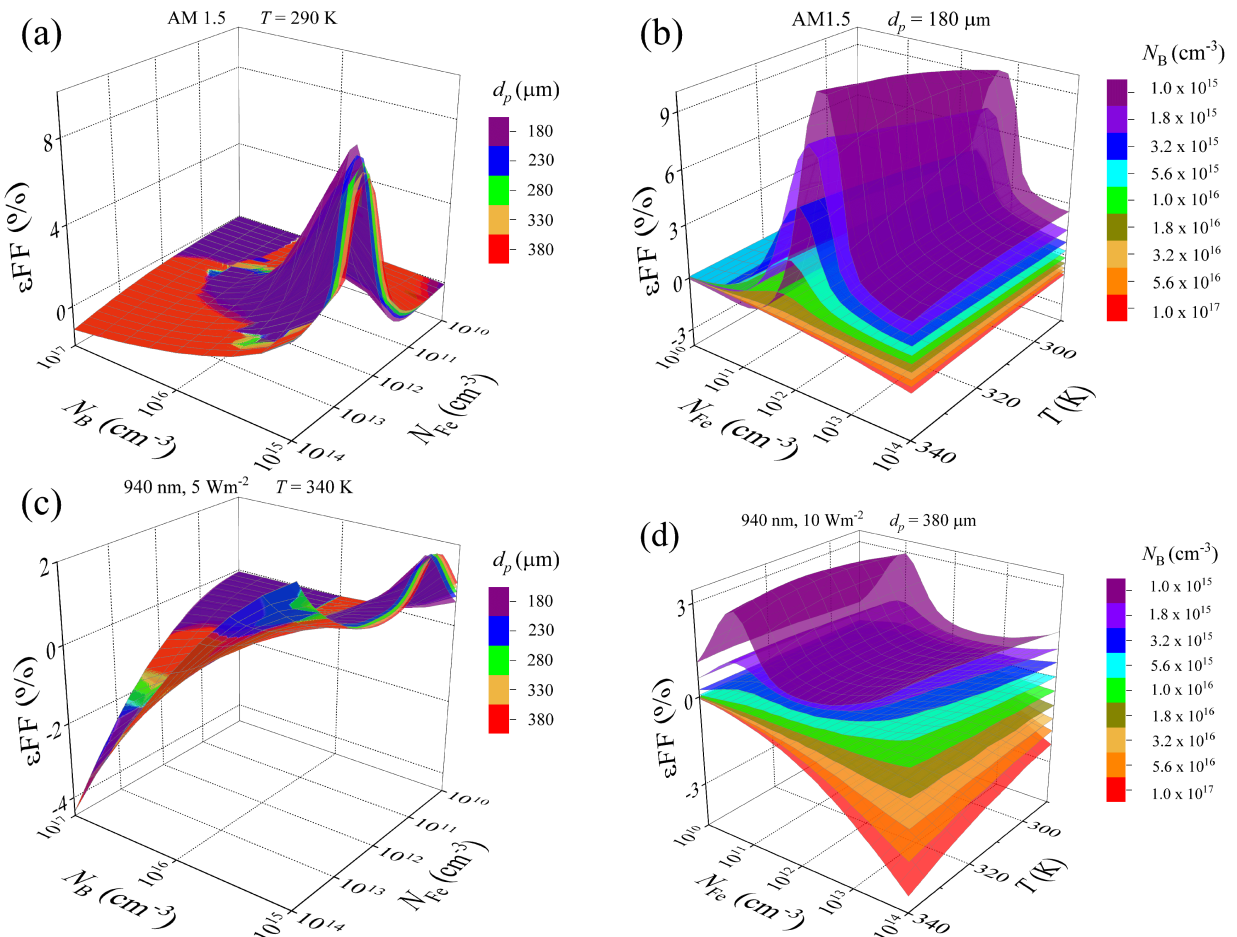


Figure 8: Relative changes in fill factor caused by a complete dissociation of Fe_xB_s pairs as a function of iron concentration and doping level (panels a and c) or temperature (b, d). Illumination: AM1.5 (a, b), 940 nm 5 W m^{-2} (c), 940 nm 10 W m^{-2} (d). T, K : 290 (a), 340 (c). $d_p, \mu\text{m}$: 180 (b), 380 (d). Different surfaces correspond to different base depths (a, c) and doping levels (b, d).

- [23] J. Schmidt, D. Macdonald, Recombination activity of iron-gallium and iron-indium pairs in silicon, *J. Appl. Phys.* 97 (2005) 113712.
- [24] M. Goodarzi, R. A. Sinton, H. Jin, P. Zheng, W. Chen, Q. Wang, D. Macdonald, Accuracy of interstitial iron measurements on p-type multicrystalline silicon blocks by quasi-steady-state photoconductance, *IEEE J. Photovolt.* 7 (2017) 1216–1223.
- [25] O. Olikh, V. Kostylyov, V. Vlasiuk, R. Korkishko, Y. Olikh, R. Chupryna, Features of FeB pair light-induced dissociation and repair in silicon n+p+p+ structures under ultrasound loading, *J. Appl. Phys.* 130 (2021) 235703.
- [26] S. Herlufsen, D. Macdonald, K. Bothe, J. Schmidt, Imaging of the interstitial iron concentration in crystalline silicon by measuring the dissociation rate of iron–boron pairs, *Phys. Status Solidi RRL* 6 (2012) 1–3.
- [27] O. Olikh, Relationship between the ideality factor and the iron concentration in silicon solar cells, *Superlattices Microstruct.* 136 (2019) 106309.
- [28] O. Olikh, O. Lozitsky, O. Zavhorodnii, Estimation for iron contamination in si solar cell by ideality factor: Deep neural network approach, *Prog. Photovoltaics Res. Appl.* 30 (2022) 648–660.
- [29] J. Schmidt, Effect of dissociation of iron–boron pairs in crystalline silicon on solar cell properties, *Progress in Photovoltaics: Research and Applications* 13 (2005) 325–331.
- [30] D. H. Macdonald, L. J. Geerligs, A. Azzizi, Iron detection in crystalline silicon by carrier lifetime measurements for arbitrary injection and doping, *J. Appl. Phys.* 95 (2004) 1021–1028.
- [31] M. A. Green, Improved silicon optical parameters at 25°C , 295 K and 300 K including temperature coefficients, *Prog. Photovoltaics Res. Appl.* 30 (2022) 164–179.
- [32] T. Niewelt, B. Steinhauser, A. Richter, B. Veith-Wolf, A. Fell, B. Hammann, N. Grant, L. Black, J. Tan, A. Youssef, J. Murphy, J. Schmidt, M. Schubert, S. Glunz, Reassessment of the intrinsic bulk recombination in crystalline silicon, *Sol. Energ. Mat. Sol.* 235 (2022) 111467.
- [33] L. E. Black, D. H. Macdonald, On the quantification of auger recombination in crystalline silicon, *Sol. Energ. Mat. Sol.* 234 (2022) 111428.

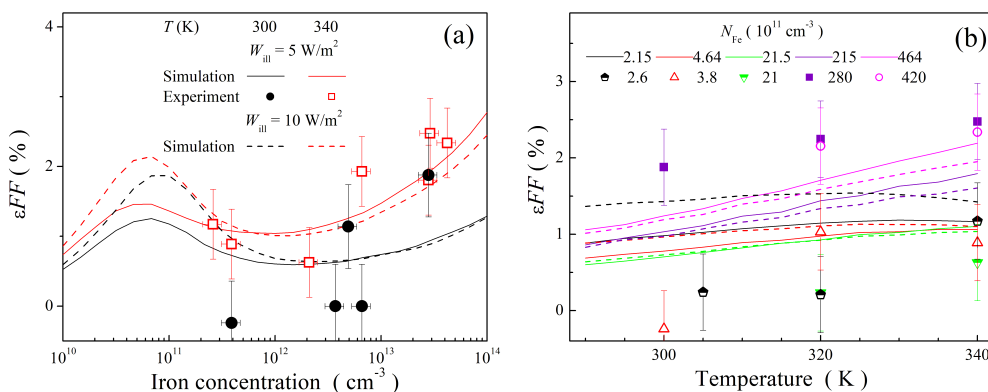


Figure 9: Relative changes in fill factor caused by a complete dissociation of Fe_3B_s pairs as a function of iron concentration (a) and temperature (b) for SSC with $d_p = 380 \mu\text{m}$ and $N_B = 1.36 \times 10^{15} \text{ cm}^{-3}$ in the case of monochromatic (940 nm) illumination. The marks are the experimental results, the lines are the simulation results. W_{ill} , Wm^{-2} : 5 (marks and solid lines), 10 (dotted lines). Different lines and marks correspond to different temperatures (a) or N_{Fe} values (b) — see legends.

- [34] A. Fell, K. R. McIntosh, P. P. Altermatt, G. J. M. Janssen, R. Stangl, A. Ho-Baillie, H. Steinkemper, J. Greulich, M. Müller, B. Min, K. C. Fong, M. Hermle, I. G. Romijn, M. D. Abbott, Input parameters for the simulation of silicon solar cells in 2014, *IEEE J. Photovolt.* 5 (2015) 1250–1263.
- [35] M. Burgelman, P. Nollet, S. Degraeve, Modelling polycrystalline semiconductor solar cells, *Thin Solid Films* 361–362 (2000) 527–532.
- [36] T. K. Joshi, G. Sharma, Y. R. Sharma, A. S. Verma, Spectroscopic screening and performance parameters of hybrid perovskite ($\text{ch}_3\text{ch}_2\text{ph}_3\text{pbI}_3$) using wien2k and scaps-1d, *Phys. B Condens. Matter* 682 (2024) 415793.
- [37] B. K. Ravidas, A. Das, S. K. Agnihotri, R. Pandey, J. Madan, M. K. Hossain, M. K. Roy, D. Samajdar, Design principles of crystalline silicon/csgei3 perovskite tandem solar cells using a combination of density functional theory and scaps-1d frameworks, *Sol. Energ. Mat. Sol.* 267 (2024) 112688.
- [38] H. Liu, L. Xiang, Q. Liu, P. Gao, Y. Zhang, S. Li, F. Gao, Toward high-performance htl-free all-perovskite tandem solar cells: Scaps simulation, *IEEE J. Photovolt.* 14 (2024) 59–64.
- [39] L. You, X. Zhang, Q. Ma, W. Zhu, J. Wu, Optimization of electron transport layer-free $\text{cs}_2\text{tibr}_6/\text{masnbr}_3$ laminated structure perovskite solar cells by scaps-1d simulation, *Phys. Status Solidi A* 220 (2023) 2300071.
- [40] A. Ait Abdelkadir, M. Sahal, Theoretical development of the czts thin-film solar cell by scaps-1d software based on experimental work, *Materials Science and Engineering: B* 296 (2023) 116710.
- [41] J. Liang, Y. Wang, Y. Zhang, X. Liu, J. Lin, Construction of perovskite homojunction for highly efficient perovskite solar cells by scaps-1d, *Materials Science and Engineering: B* 301 (2024) 117196.
- [42] M. Abdulmalik, E. Danladi, Influence of perovskite thickness on the performance of silver-doped nznbr_3 perovskite solar cells using scaps software, *Semiconductor Physics, Quantum Electronics & Optoelectronics* 26 (2023) 321–331.
- [43] R. Pässler, Dispersion-related description of temperature dependencies of band gaps in semiconductors, *Phys. Rev. B* 66 (2002) 085201.
- [44] D. Yan, A. Cuevas, Empirical determination of the energy band gap narrowing in p^+ silicon heavily doped with boron, *J. Appl. Phys.* 116 (2014) 194505.
- [45] R. Couderc, M. Amara, M. Lemiti, Reassessment of the intrinsic carrier density temperature dependence in crystalline silicon, *J. Appl. Phys.* 115 (2014) 093705.
- [46] M. A. Green, Intrinsic concentration, effective densities of states, and effective mass in silicon, *J. Appl. Phys.* 67 (1990) 2944–2954.
- [47] W. O'Mara, R. Herring, L. Hant, *Handbook of semiconductor silicon technology*, Noyes Publications, New Jersey, USA, 1990.
- [48] D. Klaassen, A unified mobility model for device simulation — I. model equations and concentration dependence, *Solid-State Electron.* 35 (1992) 953–959.
- [49] P. P. Altermatt, J. Schmidt, G. Heiser, A. G. Aberle, Assessment and parameterisation of Coulomb-enhanced Auger recombination coefficients in lowly injected crystalline silicon, *J. Appl. Phys.* 82 (1997) 4938–4944.
- [50] W. Wijaranakula, The reaction kinetics of iron–boron pair formation and dissociation in p-type silicon, *J. Electrochem. Soc.* 140 (1993) 275–281.
- [51] J. D. Murphy, K. Bothe, M. Olmo, V. V. Voronkov, R. J. Falster, The effect of oxide precipitates on minority carrier lifetime in p-type silicon, *J. Appl. Phys.* 110 (2011) 053713.
- [52] F. E. Rougieroux, C. Sun, D. Macdonald, Determining the charge states and capture mechanisms of defects in silicon through accurate recombination analyses: A review, *Sol. Energy Mater. Sol. Cells* 187 (2018) 263 – 272.
- [53] A. A. Istratov, H. Hieslmair, E. Weber, Iron and its complexes in silicon, *Applied Physics A: Materials Science & Processing* 69 (1999) 13–44.
- [54] B. B. Paudyal, K. R. McIntosh, D. H. Macdonald, Temperature dependent electron and hole capture cross sections of iron-contaminated boron-doped silicon, in: 2009 34th IEEE Photovoltaic Specialists Conference (PVSC), pp. 001588–001593.
- [55] O. Olikh, V. Kostylovy, V. Vlasuk, R. Korkishko, R. Chupryna, Intensification of iron–boron complex association in silicon solar cells under acoustic wave action, *J. Mater. Sci.: Mater. Electron.* 33 (2022) 13133–13142.

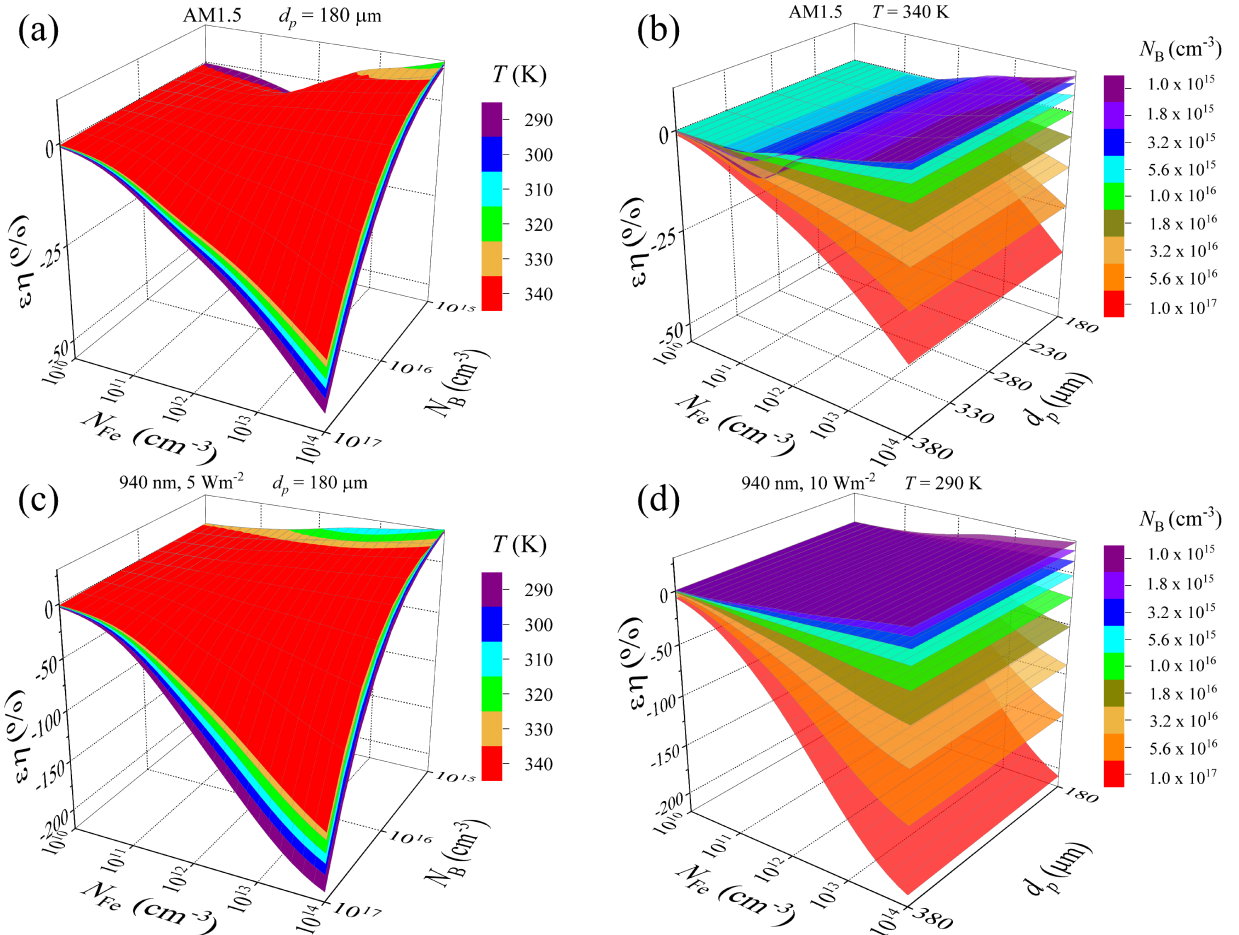


Figure 10: Relative changes in SSC efficiency caused by a complete dissociation of Fe_iB_s pairs as a function of iron concentration and doping level (panels a and c) or base depth (b, d). Illumination: AM1.5 (a, b), 940 nm 5 W m^{-2} (c), 940 nm 10 W m^{-2} (d). T, K : 290 (d), 340 (b). $d_p, \mu\text{m}$: 180 (a, c). Different surfaces correspond to different temperatures (a, c) and doping levels (b, d).

- [56] D. Yang (Ed.), *Handbook of Photovoltaic Silicon*, Springer Berlin, Heidelberg, first edition, 2019.
- [57] A. Goetzberger, J. Knobloch, B. Voss, *Crystalline Silicon Solar Cells*, Wiley, 1998.
- [58] M. A. Green, Solar cell fill factors: General graph and empirical expressions, *Solid-State Electron.* 24 (1981) 788–789.
- [59] M. A. Green, Accuracy of analytical expressions for solar cell fill factors, *Sol. Cells* 7 (1982) 337–340.
- [60] K. Bothe, D. Hinken, R. Brendel, Extended ff and voc parameterizations for silicon solar cells, *IEEE J. Photovolt.* 13 (2023) 787–792.

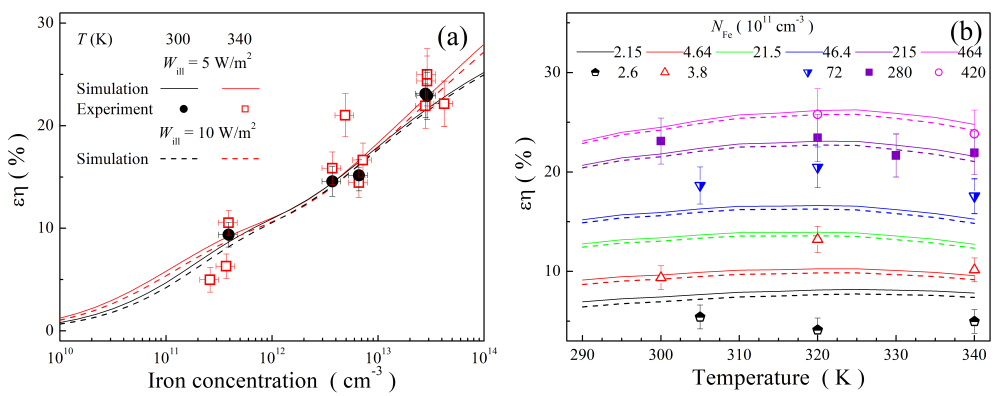


Figure 11: Relative changes in SSC efficiency caused by a complete dissociation of Fe_iB_s pairs as a function of iron concentration (a) and temperature (b) for SSC with $d_p = 380 \mu\text{m}$ and $N_{\text{B}} = 1.36 \times 10^{15} \text{ cm}^{-3}$ in the case of monochromatic (940 nm) illumination. The marks are the experimental results (divided by factor $C_{\text{cor}} = 1.4$), the lines are the simulation results. W_{ill} , W m^{-2} : 5 (marks and solid lines), 10 (dotted lines). Different lines and marks correspond to different temperatures (a) or N_{Fe} values (b) — see legends.